INSTITUTE OF PHYSICS PUBLISHING and INTERNATIONAL ATOMIC ENERGY AGENCY NUCLEAR FUSION

Nucl. Fusion **42** (2002) 1029–1038 PII: S0029-5515(02)39139-7

Modelling of Alfvén waves in JET plasmas with the CASTOR-K code*

D. Borba[1,2], H.L. Berk[3], B.N. Breizman[3], A. Fasoli[4,7], F. Nabais[1], S.D. Pinches[5], S.E. Sharapov[6], D. Testa[4] and contributors to the EFDA-JET Work Programme[a]

[1] Associacão EURATOM/IST, Av. Rovisco Pais, 1049-001 Lisboa, Portugal
[2] EDFA Close Support Unit, Culham Science Centre, Abingdon OX14 3DB, UK
[3] Institute for Fusion Studies, University of Texas at Austin, Austin, TX 78712, USA
[4] Plasma Science and Fusion Centre, MIT, Cambridge, Massachusetts, MA 02139, USA
[5] Max-Planck Institut für Plasmaphysik, Euratom Association, D85748 Garching, Germany
[6] Euratom/UKAEA Fusion Association, Culham Science Center, Abingdon OX14 3DB, UK
[7] CRPP-EPFL, Association EURATOM-Swiss Confederation, CH-1015 Lausanne, Switzerland

E-mail: Duarte.Borba@jet.efda.org

Received 22 January 2002, accepted for publication 10 June 2002
Published 7 August 2002
Online at stacks.iop.org/NF/42/1029

Abstract
A hybrid magnetohydrodynamic (MHD)-gyro-kinetic model CASTOR-K developed for the study of Alfvén eigenmode (AE) stability in the presence of energetic ions has been applied to the interpretation of recent measurements of Alfvén waves in JET. These include the detailed AE damping measurements performed using the AE antenna excitation system and also the observations of Alfvén cascades in strongly reversed shear scenarios at JET. The mode conversion between the AEs and kinetic Alfvén waves and the relation to the Alfvén continuum is studied and the calculated damping is compared with the experimental data. The contribution of ion cyclotron resonant heating driven minority ions to the growth rate of the novel-type mode localized around the point of zero magnetic shear is calculated. This mode is shown to be clearly linked to the ideal MHD 'Alfvén continuum', computed with the CSCAS code and consistent with the observation of a quasi-periodic pattern of upward frequency sweeping Alfvén cascades in JET.

PACS numbers: 52.55.Fa, 52.55.Pi, 52.55.Tn

1. Introduction

The understanding of plasma instabilities is of great importance for the optimization of the design and future operation of a fusion tokamak reactor [1]. Alfvén instabilities are particularly important, due to the fact that the charged fusion products' (α particle's) birth velocity is larger than the Alfvén velocity $V_A = B_0/\sqrt{4\pi\rho}$, where B_0 represents the equilibrium magnetic field and ρ the plasma mass density [2, 3]. Alfvén eigenmodes (AEs), eigenmodes of the ideal magnetohydrodynamic (MHD) incompressible equations such as toroidicity induced Alfvén eigenmodes (TAEs) [4–6] and ellipticity induced Alfvén eigenmodes (EAEs) [7], destabilized by energetic ions may redistribute α's and reduce the ignition margins of a tokamak reactor and/or cause damage to the first wall. The destabilization of AE [4–6] by the fusion-born α particles in tokamaks was first theoretically analysed in [8, 9] and experimentally observed in TFTR [10].

The study of AE destabilization by energetic ions produced by auxiliary heating, such as ion cyclotron resonant heating (ICRH) [11–13], is a valuable tool in understanding the physics issues related to Alfvén instabilities. These experiments offer the possibility of validating the models used in the extrapolation to reactor conditions [1].

The systematic passive measurements of instabilities in the Alfvén frequency range were carried out at JET, starting from 1997 [14]. The new high frequency digital recorders were able to store 4 s of magnetic fluctuation data at a sampling frequency of 1 MHz. With this system, detailed measurements of Alfvén instabilities have been done. It was observed that the ICRH driven energetic ions were able to destabilize AE at JET [15], for a wide range of plasma parameters. Under these

* This work was performed under the European Fusion Development Agreement.
[a] See appendix of the paper by Pamela J. 2000 Overview of recent JET results *Proc. IAEA Conf. on Fusion Energy (Sorrento, 2000).*

conditions, a very complex Alfvén spectrum emerged and it has been a challenge to understand all the physics issues in detail. Nevertheless, a comprehensive picture of AE destabilization by energetic ions has been established, with the aid of the AE active diagnostic [16, 17]. The present physics understanding can be summarized within the following topics: plasma equilibrium, Alfvén wave propagation, particle orbits, wave–particle interaction, energetic particle modes (EPMs), non-linear behaviour, saturation amplitude and energetic particle redistribution and losses.

The reconstruction of the plasma equilibrium is the first step and an important one in the detailed modelling of AE. Usually, an accurate reconstruction of the safety factor (q)-profile can be achieved using information from the sawteeth inversion radius or other MHD instabilities. However, the accurate equilibrium reconstruction of reversed shear scenarios at JET, obtained with the use of lower hybrid current drive, requires some further research, in particular scenarios with zero or negative current close to the axis [18]. However, using motion Stark effect (MSE) measurements [19] together with the information from MHD instabilities, reasonably accurate inverted q-profile equilibrium can be obtained.

The propagation of the Alfvén waves in toroidal plasmas is well established within the MHD framework, while both particle orbits and the wave particle interaction can be described successfully within the gyro-averaged approximation. In deep reversed shear scenarios, the orbits of energetic ions with energies in the 1 MeV range are mostly in the non-standard regime, where the precession drift frequency is comparable with the poloidal bounce/transit frequency. In this case, full orbit effects need to be retained, including non-standard potato orbits.

The study of the occurrence of EPMs in plasmas with a significant fraction of energetic ions is also crucial. EPM does not exist as an eigenmode of the plasma in the absence of energetic ions [20, 21], but can become unstable above a critical value of the fast particle pressure gradient [22, 23]. These modes have, in general, a higher fast ion instability threshold but once unstable can also have a larger impact on the confinement of energetic ions.

This paper will focus on the calculation of the AE spectrum and the mode destabilization by energetic ions. AE non-linear behaviour [24] and the effect on particle confinement will not be addressed.

The modelling of AE instabilities in JET can be carried out using the CASTOR-K code [25]. The CASTOR-K code is a hybrid model, containing a fluid part for the propagation of AE and mode conversion to kinetic Alfvén waves, and a gyro-kinetic part for the interaction of the energetic ion with AE. After the description of the CASTOR-K model and some of the recent enhancements (sections 2 and 3), the code will be used to analyse the damping of AE in Ohmic low temperature plasmas (section 4) and the AE spectrum in deep reversed shear plasmas (section 5). These results extend significantly the analysis of AE in JET plasmas reported previously [14], which focused on monotonic q-profiles and high temperature plasmas. The analysis in section 5 focuses on MHD modes localized around the point of zero magnetic shear. They are referred to as zero shear Alfvén eigenmodes (ZAEs). These modes are closely linked to multiple toroidal AEs discussed in [27] and to the EPMs associated with Alfvén cascades (see [26]). It is noteworthy that ZAE can exist in the absence of energetic particles provided that the mode frequency is sufficiently close to the TAE gap frequency. The contribution of ICRH driven minority ions to the growth rate of the mode with non-standard particle orbits, can be described using the CASTOR-K model. The calculations use the assumption that the eigenfrequency is close to the TAE gap frequency and that the eigenfunction is not significantly modified by fast particles even for the low frequency range.

2. CASTOR-K model (fluid part)

The hybrid MHD-kinetic CASTOR model [28, 29] solves the linearized resistive MHD equations in toroidal geometry, where the finite Larmor radius effects and the effect of the parallel electric field are included in the model within the complex resistivity approximation [30], and it is unchanged in relation to the previous version of the code [25].

In the ideal MHD framework, the damping of AE is dominated by continuum damping, caused by the resonant absorption of the AE energy at the Alfvén resonance [31, 6]. This is due to the fact that the propagation of MHD waves in a non-uniform plasma becomes singular at the Alfvén resonance, yielding a continuous spectrum for a bounded plasma [32]. The continuum mode wave energy is absorbed at the Alfvén resonance layer due to phase mixing of the singular waves. In hot plasmas, with the introduction of additional physics including non-ideal effects, such as finite perturbed electric field and finite Larmor radius, the Alfvén singularity is resolved. Non-ideal effects raise the order of the system of differential equations for AEs introducing new solutions, which describe short wavelength oscillations. The analysis of the higher order system of equations shows that the energy absorbed by phase mixing in ideal MHD is now converted into a new set of short wavelength modes with non-zero parallel electric field. The perturbed parallel electric field and first order finite Larmor radius of core ions give the following correction to the vorticity equation [33]:

$$\underbrace{(\vec{b}\cdot\vec{\nabla})(\nabla^2(\vec{b}\cdot\vec{\nabla})\phi)+\nabla\left(\frac{\omega^2}{V_{\mathrm{A}}^2}\nabla_\perp\phi\right)}_{\text{Ideal MHD part}}+\underbrace{\frac{3}{4}\frac{\omega^2}{V_{\mathrm{A}}^2}\rho_{\mathrm{i}}^2\nabla_\perp^4\phi}_{\text{FLR}}$$
$$+\underbrace{(1-\mathrm{i}\delta_{\mathrm{e}})\frac{\omega^2}{V_{\mathrm{A}}^2}\rho_S^2\nabla_\perp^4\phi}_{E_{||}\neq 0\text{ term}}=0,$$

with dissipation δ_{e} due to the electron. The vorticity equation has the following form in resistive MHD:

$$\underbrace{(\vec{b}\cdot\vec{\nabla})(\nabla^2(\vec{b}\cdot\vec{\nabla})\phi)+\nabla\left(\frac{\omega^2}{V_{\mathrm{A}}^2}\nabla_\perp\phi\right)}_{\text{Ideal MHD part}}$$
$$+\underbrace{(\vec{b}\cdot\vec{\nabla})\frac{\mathrm{i}\tilde{\eta}}{4\pi\omega}(\nabla_\perp^4(\vec{b}\cdot\vec{\nabla})\phi)}_{\text{Resistive term}}=0.$$

The direct comparison of the previous equations gives us the 'complex resistivity', where

$$\omega_{\mathrm{A}}=\frac{V_{\mathrm{A}}}{R_0},\qquad \rho_S=\sqrt{\frac{T_{\mathrm{e}}}{T_{\mathrm{i}}}}\rho_{\mathrm{i}}$$

and ρ_i the ion Larmor radius.

$$\tilde{\eta} = 4\pi\omega\rho_S^2\left(\frac{2\omega}{\omega_A}\right)^2\delta_e + i4\pi\omega\left(\frac{3}{4}+\frac{T_e}{T_i}\right)\rho_i^2\left(\frac{2\omega}{\omega_A}\right)^2.$$

In order to understand the behaviour of Alfvén waves in the presence of FLR and finite parallel electric field, the Alfvén spectrum can be solved within the Wentzel–Kramers–Brillouin–Jeffreys (WKBJ) approximation. The transition from the resistive Alfvén spectrum into the kinetic Alfvén spectrum can be studied by changing the usual resistivity into a general complex parameter $\tilde{\eta}$. The fast varying solutions in the radial direction can be described accurately by the phase integral in the WKBJ approximation [34] $\phi \approx e^{\pm i\phi_f}$, where

$$\frac{d\phi_f}{dr} = \sqrt{-\frac{(\vec{k}\cdot\vec{b})+\omega^2}{\tilde{\eta}\omega}}.$$

To obtain the WKBJ spectrum the following eigenvalue conditions for ω must be satisfied:

(a) no anti-Stokes line crossings $\phi_f(b) - \phi_f(a) = p\pi \rightarrow \mathrm{Im}\lfloor\phi_f(a)\rfloor < 0 \wedge \mathrm{Im}\lfloor\phi_f(b)\rfloor < 0$,
(b) one at (a) and half at (b) anti-Stokes line crossings $\phi_f(a) = -p\pi \rightarrow \mathrm{Im}\lfloor\phi_f(b)\rfloor > 0$,
(c) one at (b) and half at (a) anti-Stokes line crossings $\phi_f(b) = p\pi \rightarrow \mathrm{Im}\lfloor\phi_f(a)\rfloor > 0$,

where a, b are the boundaries.

In the generalized case of complex $\tilde{\eta}$ the spectrum rotates and the third branch disappears with the two remaining branches forming the kinetic Alfvén spectrum. The kinetic Alfvén waves corresponding to the second branch have a turning point at the Alfvén resonance giving rise to the kinetic toroidicity induced Alfvén eigenmodes (KTAEs) in toroidal geometry [35]. The first branch does not have a turning point inside the plasma and plays an important role in radiative damping of Alfvén waves. In the low shear ($s \rightarrow 0$) limit the dispersion relation for each branch takes the form

$$\frac{s+2(1+\omega^2)}{2(1+\omega^2)}\sqrt{-\frac{\omega^2+1}{\tilde{\eta}\omega}} = p\pi,$$

$$\frac{s\omega+2i(1+\omega^2)}{2\tilde{\eta}\sqrt{-(\omega^2+1)/\tilde{\eta}\omega}} = p\pi,$$

$$\left(1+\frac{s}{2}+2i\omega\right)\sqrt{-\frac{\omega^2+1}{\tilde{\eta}\omega}} = p\pi.$$

For very large values of p the dispersion relation can be simplified $\omega = \frac{1}{2}(-\tilde{\eta}p^2\pi^2 \pm \sqrt{\tilde{\eta}^2p^4\pi^4-4})$. Since p is the number of radial wave periods, $p \propto k_\perp$, one obtains $\gamma = \mathrm{Im}(\omega) \propto \tilde{\eta}k_\perp^2$, showing that within the CASTOR-K complex resistivity approximation the short wavelength waves are damped proportionally to the perpendicular radial wave number square $k_\perp^2$.

The CASTOR-K code calculates the non-ideal Alfvén spectrum using two distinct numerical algorithms. In the first procedure the linearized non-ideal MHD equations are solved as an eigenvalue problem using inverse vector interaction. In the second method the plasma response to an external antenna excitation is calculated using linear solver. The damping of the eigenmode is determined by the width of the resonance or directly from the eigenvalue. The ideal and non-ideal plasma response for a simple benchmark cylindrical equilibrium [36] is shown in figure 1. As the non-ideal complex parameter $\tilde{\eta}$ increases, the damping of the TAE [4] located inside the toroidicity induced gap in the continuum increases, causing the resonance observed in the plasma response to broaden. The break up of the continuum in a discrete set of kinetic Alfvén waves is also clearly visible in figure 1 as the non-ideal complex parameter $\tilde{\eta}$ is increased.

Numerical convergence for a JET limiter Ohmic discharge requires around 151 radial finite cubic elements and 11–17 poloidal Fourier harmonics, depending on edge q and toroidal mode number of the eigenmode. Computational resources consistent with these requirements and with a systematic comparison with the experimental data were made available in the last few years, therefore allowing the analysis presented in this paper.

Figure 2 shows the damping of $n = 1$ TAE mode as a function of the underlying plasma dissipation $\mathrm{Re}(\tilde{\eta}) \propto \delta_e$. Calculation of the damping of this mode shows that above a certain value of the underlying plasma dissipation δ_e, the damping becomes independent of the plasma dissipation δ_e and depends only on the amount of energy converted from the AE to the runaway kinetic Alfvén wave. It is, therefore, shown that in this parameter regime the CASTOR-K model reproduces the radiative damping limit.

The analysis of the dependence of the damping of the TAE on the non-ideal parameter $\tilde{\eta}$ shows the existence of three separate cases that need to be considered. The damping of the TAE mode located at the bottom of the TAE gap tends to be dominated by radiative damping, which increases with $\tilde{\eta}$. The TAE mode located at the top of the gap usually crosses the Alfvén continuum and is continuum damped. This mode has a finite damping in ideal MHD and the damping has a weak dependence on $\tilde{\eta}$. KTAE modes do not exist in the ideal MHD and the damping decreases with $\tilde{\eta}$ as shown in figure 3.

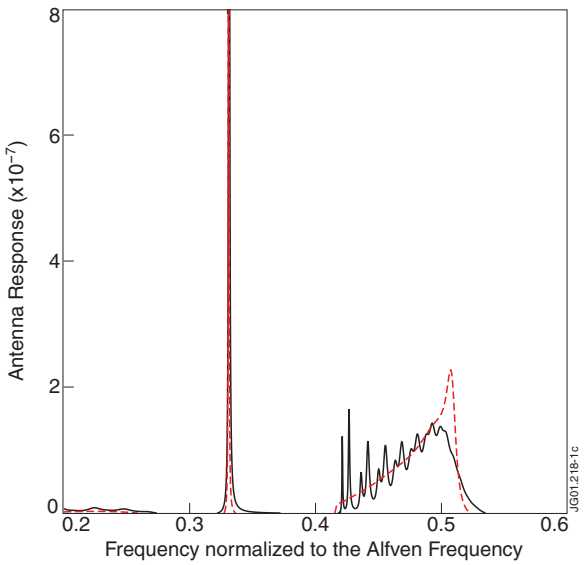

Figure 1. Ideal (red-dashed) and non-ideal (black) plasma response for a simple benchmark cylindrical equilibrium, showing the increase in damping of the TAE located inside the continuum gap and the break up of the continuum in a discrete set of kinetic Alfvén waves as the complex parameter is increased.

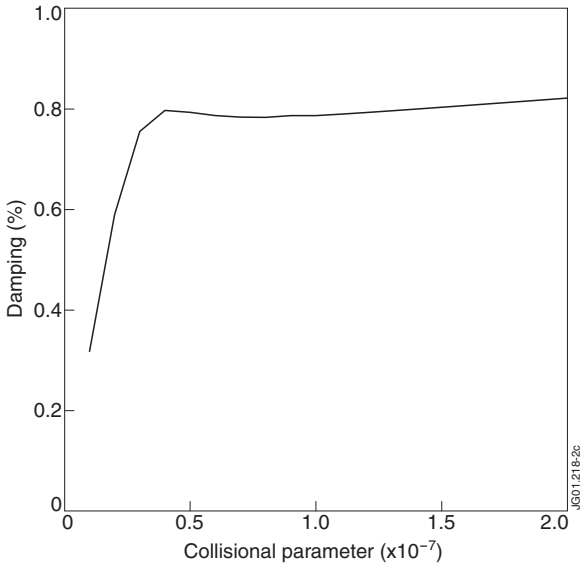

Figure 2. Damping of $n = 1$ TAE mode as a function of the underlying plasma dissipation. Above a certain value of dissipation the overall damping becomes independent of the underlying plasma dissipation, reproducing the radiative damping limit.

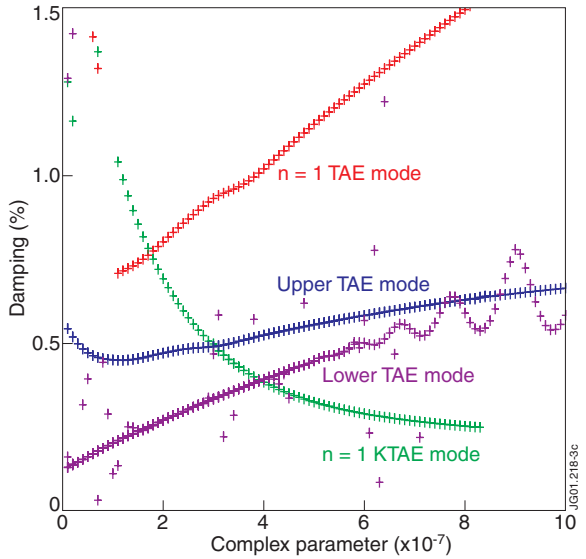

Figure 3. Damping of $n = 1$ TAE and KTAE modes as a function of the non-ideal complex parameter. The damping of the TAE mode increases with plasma pressure, directly related non-ideal complex parameter, while the damping of KTAE mode decreases with plasma pressure.

3. CASTOR-K model (gyro-kinetic part)

The gyro-kinetic part of the CASTOR-K code calculates the transfer of energy between the fast particles and the mode. This code was originally developed in order to study TAE destabilization by α particles, and later it was extended to analyse the influence of ICRH heated particles on the stability of lower frequency MHD modes.

The CASTOR-K code then calculates the contribution of the fast particles to the energy of the mode using a perturbative approach. It computes the first order perturbation on the eigenvalue due to the interaction between the wave and the energetic ion population, using the eigenfunction determined by the fluid part of the code. CASTOR-K decomposes the hot particle energy functional into poloidal bounce harmonics and integrates the contribution over the particle phase space, as seen in equation (1):

$$\delta W_{\mathrm{HOT}} = -\frac{2\pi^2}{\Omega m^2}\sum_{\sigma}\int \mathrm{d}P_\phi\,\mathrm{d}E\,\mathrm{d}\mu \times \sum_{p=-\infty}^{\infty}\frac{\partial f}{\partial E}\frac{\tau_{\mathrm{b}}|Y_p|^2(\omega - n_0\omega^*)}{\omega + n_0\omega_{\mathrm{D}} + p\omega_{\mathrm{b}}},$$
$$Y_p = \oint \frac{\mathrm{d}\tau}{\tau_{\mathrm{b}}} L^{(1)} \mathrm{e}^{\mathrm{i}p\omega_{\mathrm{b}}\tau}. \qquad (1)$$

P_ϕ represents the toroidal canonical momentum, μ the magnetic momentum, E the energy, $L^{(1)}$ the perturbed orbit Lagrangian, ω^* the diamagnetic frequency of the fast ions, ω the perturbation frequency, ω_{D} toroidal precession drift frequency and ω_{b} the poloidal bounce frequency, Ω the cyclotron frequency and m the mass of the fast ions. The imaginary part of δW_{HOT}, which represents the contribution of the energetic ions to the linear MHD eigenvalue, is related to the growth rate of the mode (γ/ω) by

$$\frac{\gamma}{\omega} = \frac{1}{2\omega^2}\frac{\mathrm{Im}[\delta W_{\mathrm{HOT}}]}{E_k}, \qquad (2)$$

where E_k is proportional to the mode energy and γ is the growth rate of the unperturbed mode, as shown in equation (2).

The six-dimensional integration in phase space is performed using both numerical and analytic methods. In the original CASTOR-K version the integration was performed using the procedure represented in table 1. The new version of the CASTOR-K code uses a modified procedure as shown in table 2. The new procedure [37] assumes that ICRH transfers energy to the fast ions only in the perpendicular direction, generating distributions with a single value of the magnetic momentum divided by energy. This allows the energy integration to be performed numerically using the two-dimensional binary search algorithm and the consequent calculation of both the real and imaginary parts of the quadratic form δW_{HOT}.

Table 1.

Variable		Integration process	
α	Gyro-angle	Analytical	Gyro-average
θ	Poloidal angle	Numerical	Fourier transform
ϕ	Toroidal angle	Analytical	Fourier decomposition
E	Energy	Analytical	Pole integration
μ/E	Magnetic moment	Numerical	Binary search
P_ϕ	Toroidal momentum	Numerical	Binary search

Table 2.

Variable		Integration process	
α	Gyro-angle	Analytical	Gyro-average
θ	Poloidal angle	Numerical	Fourier transform
ϕ	Toroidal angle	Analytical	Fourier decomposition
E	Energy	Numerical	Binary search
μ	Magnetic moment	Analytical	ICRH distribution
P_ϕ	Toroidal momentum	Numerical	Binary search

The binary search algorithm is important, because small 'resonance' areas in phase space dominate the wave–particle interaction. This algorithm allows consecutive mesh refinements in areas where the wave–particle interaction is strongest. In an initial step the algorithm surveys the entire phase space, and in the following steps the mesh is refined using evaluation, ordering and storing procedures. The convergence is found to be linear in the number of steps and adequate in most practical applications.

4. Alfvén spectrum excited by external antenna in Ohmic plasmas

The calculated continuum and radiative damping were found to be very sensitive to the experimental profiles, in particular the density and safety factor profiles. However, using the destabilization of the sawtooth as evidence of the appearance of the $q = 1$ surface in the centre of the plasma, a relatively accurate q-profile can be reconstructed for (shot #51158 at $t = 6$ s) using the codes EFIT [38] and HELENA [39]. The density profile can also be reconstructed accurately using the data from the LIDAR Thomson scattering and microwave interferometer diagnostics.

The calculated frequency and damping is compared with the measurements using the AE active excitation diagnostic. In this discharge, the probing frequency is scanned with the frequency range calculated to be in the vicinity of the toroidicity induced gap. Once the system detects a resonance, it follows the mode measuring the frequency and damping as a function of time. In this discharge two $n = 1$ modes are found in the TAE gap. The MHD model also shows the existence of two $n = 1$ TAE modes in the gap in agreement with the experiments, and the model is able to reproduce the frequency of the AEs with high accuracy as shown in figure 4. The Alfvén continuous spectrum, and frequency of the eigemodes found in the TAE gap for discharge #51158 for the time slice $t = 6.5$ s is shown in figure 5. The eigenfunctions calculated by the CASTOR for this discharge are shown in figures 6 and 7. The radial plasma displacement is represented as a function of the normalized magnetic poloidal flux $s = \sqrt{\psi/\psi_0}$, which is approximately equivalent to the normalized plasma minor radius (r/a). The upper frequency ($f = 150$–170 kHz) TAE mode, shown in figure 6, has no parity inversion, in contrast with the lower frequency ($f = 120$–130 kHz) TAE mode which has a parity inversion at $s = 0.75$ as shown in figure 7. The calculated damping for the lower frequency ($f = 120$–130 kHz) TAE mode for this discharge is found

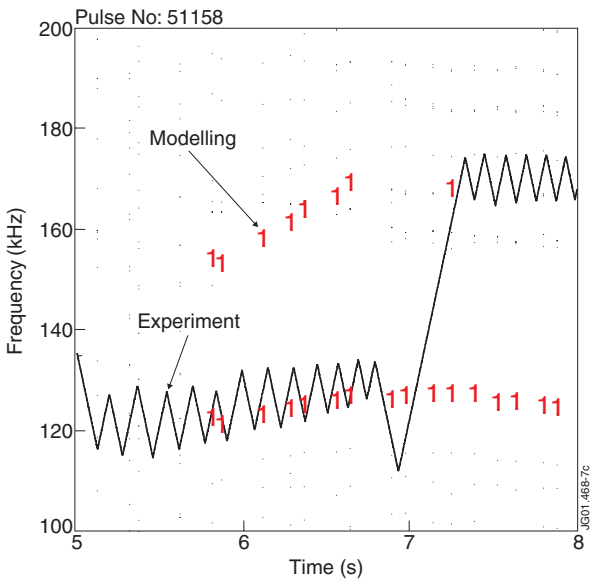

Figure 4. Frequency of two $n = 1$ TAE modes (lower TAE, upper TAE) measured using the active AE excitation diagnostic at JET (continuous line), compared with the frequency calculated using the CASTOR code (symbol 1) for discharge #51158. The MHD model reproduces the experimentally observed frequency with high accuracy.

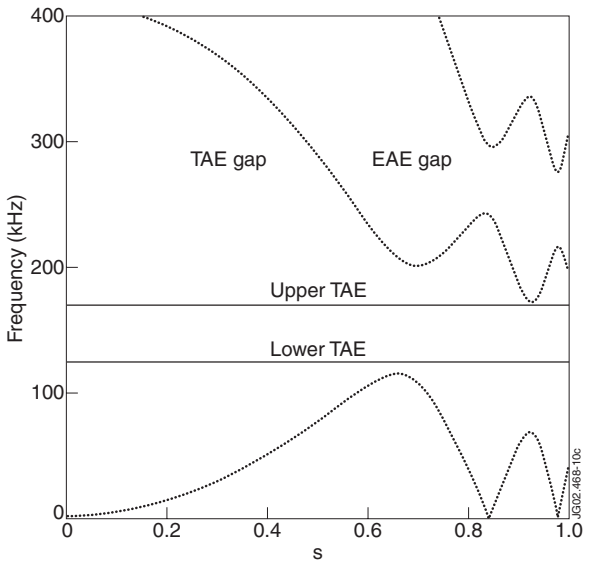

Figure 5. Alfvén continuous spectrum, and frequency of the eigenmodes with toroidal mode number $n = 1$ found in the TAE gap for discharge #51158 for the time slice $t = 6.5$ s.

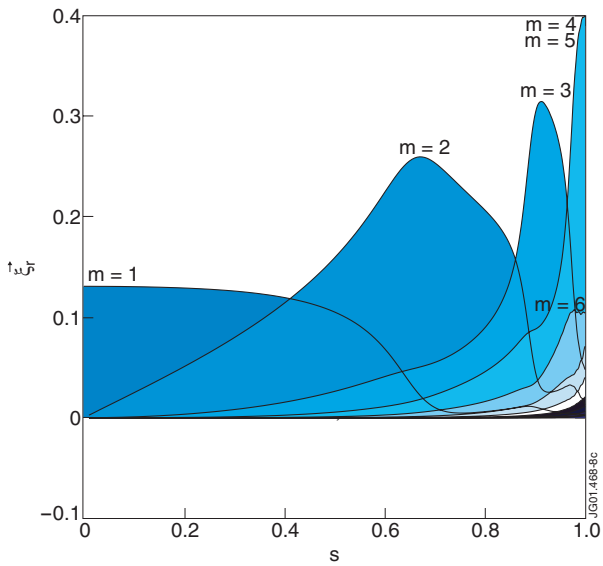

Figure 6. Radial plasma displacement as a function of the square root of the normalized poloidal magnetic flux of the upper frequency ($f = 150$–170 kHz) $n = 1$ TAE mode calculated using the CASTOR code for discharge #51158.

to be 0.5–1%, a factor of 2 smaller than the measured damping of 1–2% as shown in figure 8. This study shows that the Alfvén wave mode conversion model implemented in the CASTOR-K code underestimates the measured damping by a factor 2. This discrepancy cannot be attributed to uncertainties in the density and q-profile. This is confirmed by the sensitivity studies and the fact that the measured frequency for two eigenmodes provides a strong constraint in the sensitivity analysis. This disagreement is not unexpected taking into account that the model is based on the simplifying assumptions of the complex resistive approximation described previously [30]. However, if mode conversion were not included in the CASTOR-K model the discrepancy would be much larger, therefore, the importance of mode conversion in the analysis of the damping of TAEs. This result emphasizes the importance of mode conversion in addition to continuum damping in the overall damping of AE in JET Ohmic plasmas, as shown in figure 3.

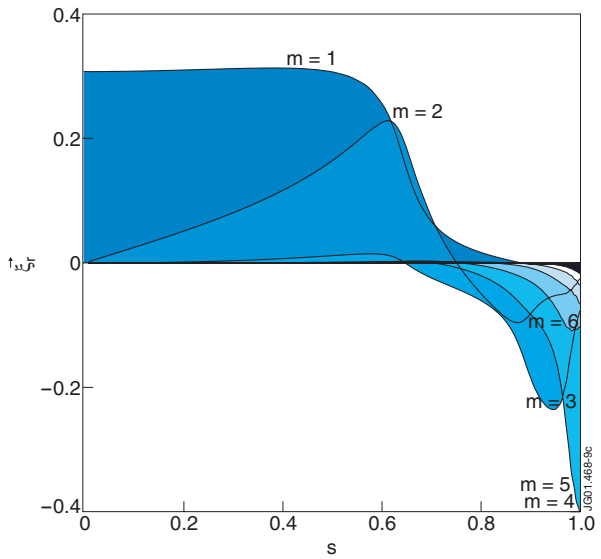

Figure 7. Radial plasma displacement as a function of the square root of the normalized poloidal magnetic flux of the lower frequency ($f = 120$–130 kHz) $n = 1$ TAE mode calculated using the CASTOR code for discharge #51158.

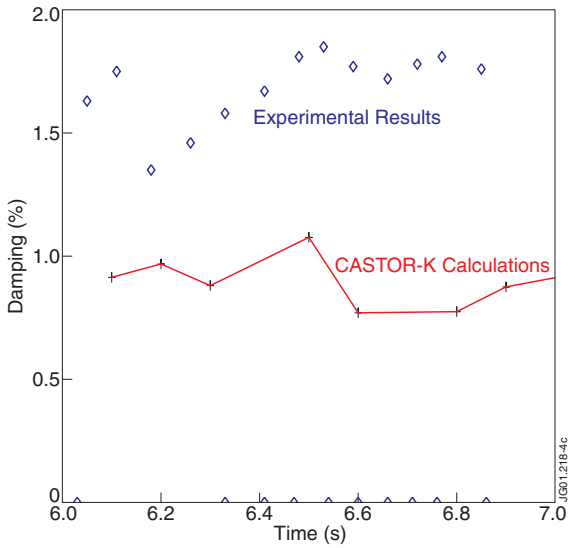

Figure 8. Comparison between the TAE damping measured by the active AE antenna system and the damping calculated using the CASTOR-K code for shot #51158, for the lower frequency ($f = 120$–130 kHz) TAE mode. The calculated damping for the lower TAE mode for this discharge is found to be 0.5–1%, a factor of 2 smaller than the measured damping of 1–2%.

5. Alfvén spectrum in deep reversed shear plasmas

A detailed analysis of the Alfvén spectrum in deep reversed shear plasmas is carried out using an equilibrium reconstruction obtained with the MSE diagnostic at JET for discharge #49382. The reconstructed q-profile is strongly reversed with q on axis $q_0 \sim 6.0$ and $q_{\min} \sim 2.5$ located around $r(q_{\min}) \sim 0.62$ minor radius. The Alfvén spectrum as calculated with the fluid part of the CASTOR-K code is quite complex and a number of eigenmodes have been found in the vicinity of the TAE gap. Among these, only three AEs with damping rate γ/ω less than 3% were found. The Alfvén continuous spectrum, the frequency and approximate location of the eigenmodes found in the vicinity of the TAE gap are shown in figure 9. A core localized EAE was found with frequency just above the TAE gap. The radial plasma displacement of the core localized EAE eigenfunction, represented as a function of the square root of the normalized magnetic poloidal flux, is shown in figure 10. A global TAE exists in the middle of the TAE gap with small damping. The radial plasma displacement of the global TAE, represented as a function of the square root of the normalized magnetic poloidal flux, is shown in figure 11. In addition, a localized eigenmode was found located in radius at the position of the minimum of q with frequency below the TAE mode frequency.

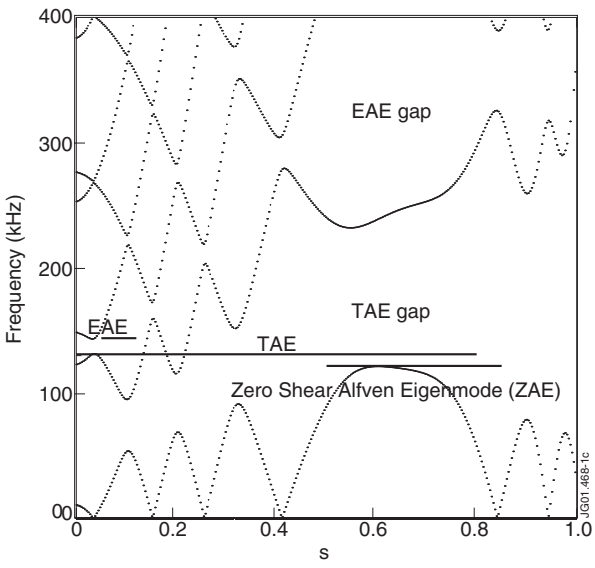

Figure 9. Alfvén continuous spectrum, the frequency and approximate location of the eigemodes, with toroidal mode number $n = 1$, found in the vicinity of the TAE gap for the deep reversed shear discharge #49382. A global TAE exists in the middle of the TAE gap and a core localized EAE is found with frequency just above the TAE gap. In addition, a localized eigenmode referred to in the paper as ZAE is found located in radius at the position of the minimum of q with frequency below the TAE mode frequency.

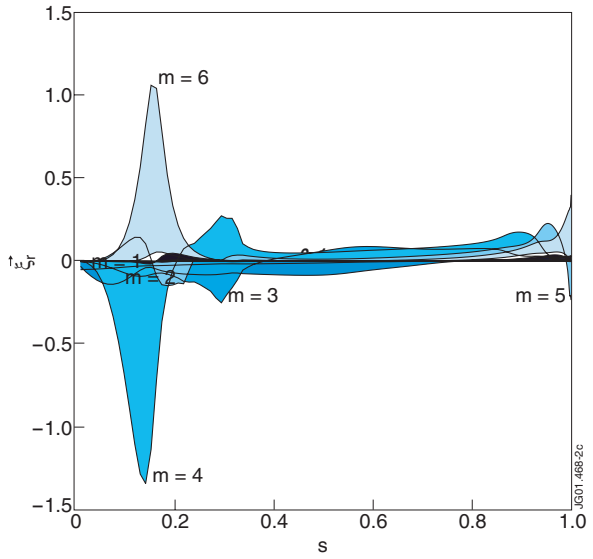

Figure 10. Radial plasma displacement as a function of the square root of the normalized poloidal magnetic flux of a $n = 1$ core localized EAE with frequency just above the TAE gap for the deep reversed shear discharge #49382.

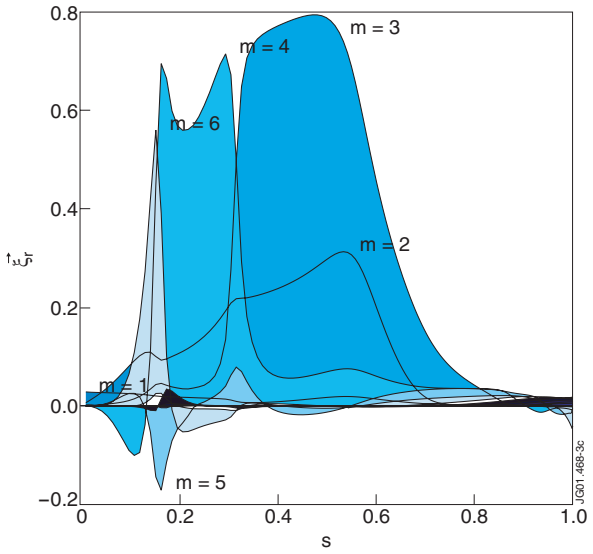

Figure 11. Radial plasma displacement as a function of the square root of the normalized poloidal magnetic flux of a global $n = 1$ TAE that exists in the middle of the TAE gap for the deep reversed shear discharge #49382.

The radial plasma displacement of this localized eigenmode, represented as a function of the square root of the normalized magnetic poloidal flux, is shown in figure 12. The analysis of the frequency dependence on the evolution of q for these modes was carried out by varying the value of the minimum of q from 2.0 to 3.0. It was found that the frequency of the mode located at the minimum of q was clearly linked with the tip of the Alfvén continuum spectrum:

$$\frac{\mathrm{d}}{\mathrm{d}r}(k_{||}V_{\mathrm{A}}) = 0$$

at the same position as shown in figure 13. The transition from the low shear TAE mode [27] composed of two dominant

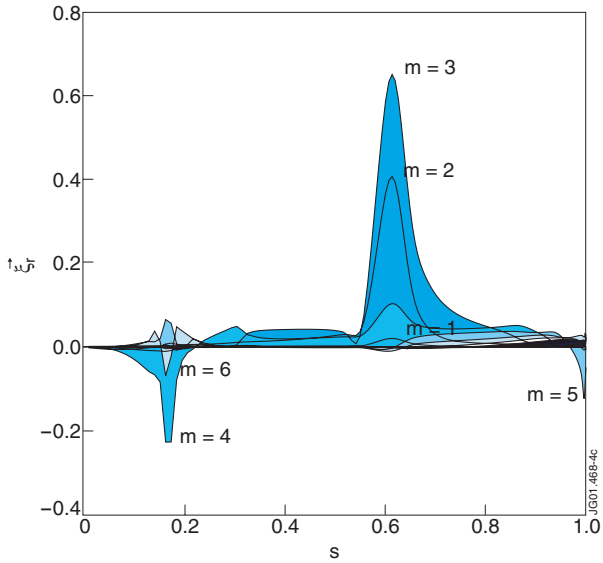

Figure 12. The radial plasma displacement as a function of the square root of the normalized poloidal magnetic flux of a localized $n = 1$ eigenmode (ZAE) found localized in radius at the position of the minimum of q, for the value of $q_{\mathrm{min}} = 2.5$ with mode frequency $f_{\mathrm{mode}} = 121$ kHz, with frequency below the TAE mode frequency for the deep reversed shear discharge #49382.

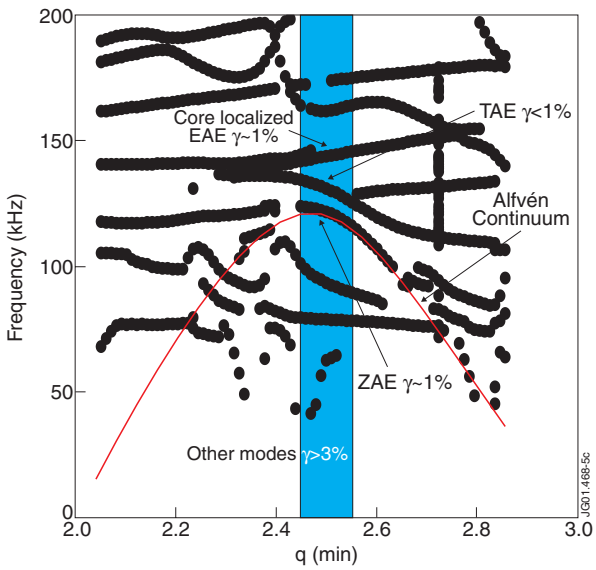

Figure 13. Analysis of the frequency dependence on the evolution of q of the Alfvén spectrum by varying the value of the minimum of q from 2.0 to 3.0. The $n = 1$ Alfvén continuum at the position of q_{min} is represented by the red line. The eigenmodes with the calculated damping smaller than 1% are also indicated in the figure. The frequency of the mode located at the minimum of q (ZAE) is clearly linked with the continuum spectrum at the same position.

poloidal harmonics ($m = 2, m = 3$), into a 'cylindrical' mode [26] dominated by a single poloidal harmonic is clearly visible in figure 14, as the mode frequency decreases and moves further away from the TAE gap. We conclude therefore that the Alfvén cascades observed in JET plasma with the deep reversed q-profiles can be interpreted as a ZAE located at the position of q_{min} and whose frequency is close to the Alfvén continuous spectrum at the position of q_{min}. This

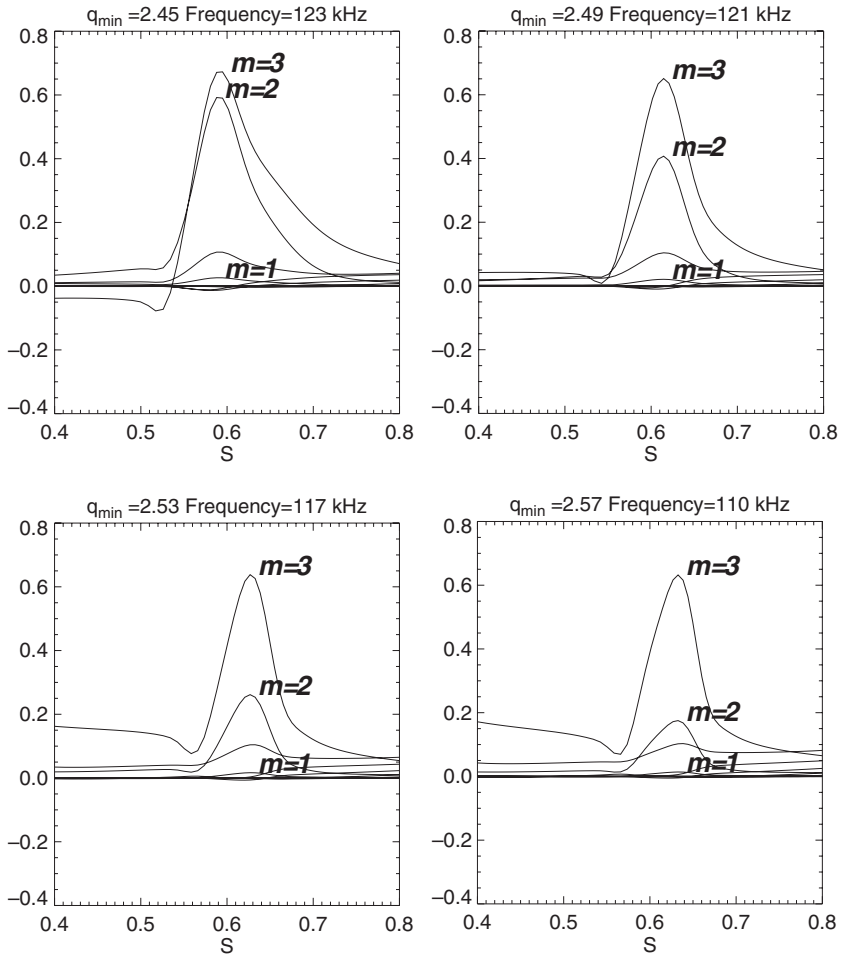

Figure 14. Detail of the radial plasma displacement as a function of the square root of the normalized poloidal magnetic flux ($s = 0.4$–0.8) of a localized $n = 1$ eigenmode (ZAE) found localized in radius at the position of the minimum of q, for the values of $q_{\min} = 2.45$, 2.49, 2.53 and 2.57 with mode frequency $f_{\text{mode}} = 123$, 121, 117 and 110 kHz. The transition from the low shear TAE mode composed of two dominant poloidal harmonics ($m = 2, m = 3$) into a 'cylindrical' mode dominated by a single poloidal harmonic is clearly visible as the mode frequency decreases and moves further away from the TAE gap.

mode exists in the absence of energetic ions, provided that the mode frequency is sufficiently close to the TAE gap. In the case of the frequency being far away from the TAE gap the ZAE mode existence requires finite pressure of energetic ions. However, the frequency of the mode remains linked with the Alfvén continuum and the frequency changes within a timescale consistent with the q-profile evolution [40], in contrast to the EPM where the frequency change is set by the characteristic inverse growth rate timescale [22] ($\sim 100\tau_{\text{A}}$).

In order to evaluate the stability of these modes in the presence of ICRH accelerated minority ions, it is necessary to take into account the orbits of high energy ions in deep reversed shear plasmas in some detail. In the small banana limit the particle orbits can be classified into passing and trapped particles. In the case of high energy ions, where the banana width is comparable with the plasma minor radius the topology of the orbits is more complicated. Considering only the region in phase space relevant to ICRH accelerated minority ions the orbits can be classified in two groups, banana orbits and potato orbits. Due to the small current in the plasma core, a large fraction of ions with energies in the MeV range are in the potato regime and the toroidal precession drift frequency is comparable with the poloidal bounce frequency. Therefore, in the calculation of the destabilization of AEs, it is crucial to take into account the contribution of non-standard orbits. For the configuration considered, it was found that the main destabilizing influence is dominated by the trapped banana orbits, while most particles in the potato regime have a stabilizing influence. Figure 15 represents the energy exchange between the energetic particles and the eigenmode localized around the position of $q_{\min}$ as a function of the energy and the toroidal canonical momentum. The stabilizing influence of mainly non-standard potato orbits is represented in red, while the destabilizing influence of the trapped banana orbits is represented in blue. It is also clearly seen in figure 15 that the relatively narrow resonant regions in phase space dominate the interaction between the mode and the energetic ions. These are the regions at which the CASTOR-K code uses the mesh refinement described in section 3 in order to improve the accuracy of the calculation. A stability diagram for the least damped eigenmodes calculated by the CASTOR-K code for the equilibrium of the deep reversed shear discharge #49382 is shown in figure 16. The TAE mode requires lower fast ion β for instability because it has lower continuum damping. The ZAE

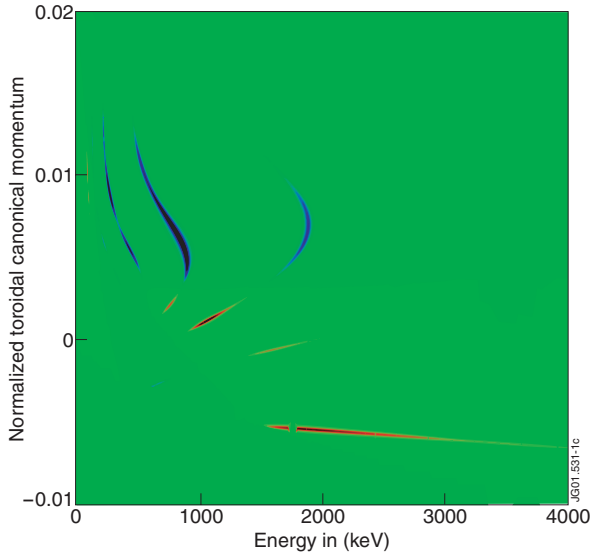

Figure 15. Energy exchange between the energetic particles and the eigenmode localized around the position of $q_{\min}$ (ZAE) as a function of the energy and the toroidal canonical momentum. The stabilizing influence of mainly non-standard orbits is represented in red, while the destabilizing influence of the trapped banana orbits is represented in blue.

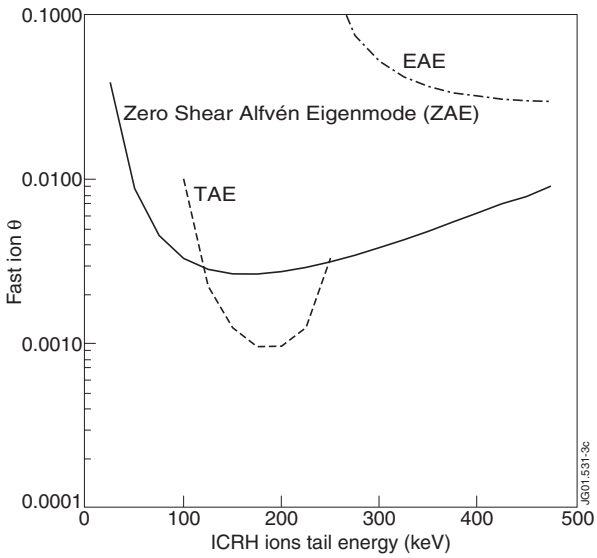

Figure 16. Stability diagram for the least damped eigenmodes calculated by the CASTOR-K code for the equilibrium of the deep reversed shear discharge #49382. The TAE mode requires lower fast ion β for instability but the mode localized at the minimum of q (ZAE) is the most unstable for a wide range of parameters.

mode localized at the minimum of q is the most unstable mode for a wider range of parameters, because the TAE mode has a stronger damping from the high energy generated ICRF ions in the potato regime. The overall stability analysis performed by the CASTOR-K code, where the ZAE mode is shown to be the most likely unstable mode, is consistent with the experimental observation that Alfvén cascades are the dominant Alfvén instability in plasmas with deep reversed q-profiles.

Detailed comparison of the ZAE mode frequency pattern of the Alfvén cascades and Alfvén continuum located at

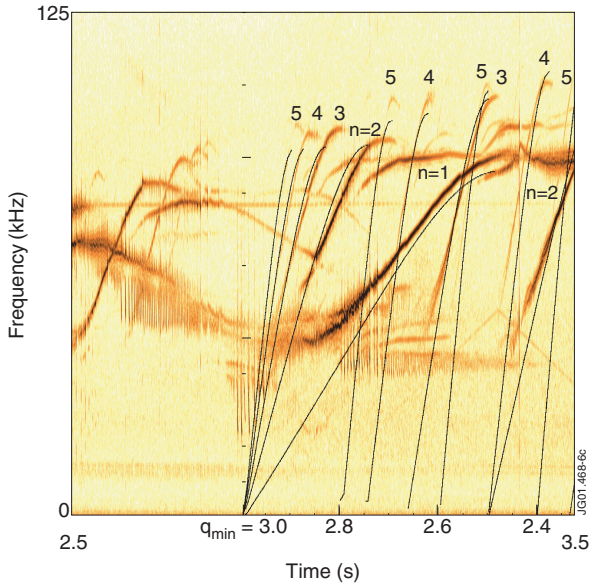

Figure 17. Spectrogram of the magnetic fluctuations showing the presence of Alfvén cascades common in deep reversed shear discharges with ICRH. The calculated frequency of the Alfvén continuum at the position of $q_{\min}$ modified by $f_{\text{corrected}} = f_{\text{continuum}}(1 - 0.2/n)$, where n is the toroidal mode number, is shown for comparison.

$q_{\min}$ has been performed. The Alfvén continuum at $q_{\min}$ behaviour is qualitatively the same as the Alfvén cascades if only cases where the Alfvén continuum has a maximum at the $q_{\min}$ surface are considered. This is consistent with the existence of the mode near the TAE gap calculated by the CASTOR-K code. Furthermore, better agreement is obtained by including a reduction of the mode frequency by a factor inversely proportional to the toroidal mode number (n), $f_{\text{corrected}} = f_{\text{continuum}}(1 - 0.2/n)$, as shown in figure 17.

6. Conclusions

The CASTOR-K model for the radiative damping of TAE modes has been compared with the damping measurements performed at JET, using the AE active eigenmode excitation system. The mode frequency in Ohmic plasmas is reproduced by the ideal MHD model with great accuracy. The calculated damping was found to be around a factor of 2 smaller than the measured damping. This disagreement is consistent with the simplifying assumptions of the complex resistive approximation implemented in the CASTOR-K code. However, these results show the importance of mode conversion and continuum damping in the overall damping of AE in JET Ohmic plasmas.

In deep reversed shear scenarios, a mode localized at the position of the minimum of the safety factor q, referred to as ZAE, was calculated by the CASTOR-K code. The ZAE was found to exist in the ideal framework only if the frequency of the mode is close to the frequency of the TAE gap. Stability calculations show that the ZAE is the most unstable eigenmode for a wide range for parameters consistent with the experimental observation of Alfvén cascades. The frequency pattern of the Alfvén cascades is qualitatively in

agreement with the time evolution of the Alfvén continuum at the location of $q_{\min}$ which is linked to the frequency of the mode calculated by the CASTOR-K code. Measurements of these Alfvén instabilities are used to solve the inverse problem of identifying the plasma parameters, especially the minimum of the safety factor ($q_{\min}$) shown in figure 17.

Acknowledgments

This work has been carried out within the framework of the contract of association between the European Atomic Energy Community and Instituto Superior Técnico and has also received financial support from Fundação para a Ciencia e a Tecnologia (FCT). The content of the publication is the sole responsibility of the authors and it does not necessarily represent the views of the Commission of the European Union or their services.

References

[1] ITER Physics Basis (chapter 5) 1999 *Nucl. Fusion* **39** 2471
[2] Rosenbluth M.N. and Rutherford P.H. 1975 *Phys. Rev. Lett.* **34** 1428
[3] Mikhailovskii A.B. 1975 *Sov. Phys. JETP* **41** 890
[4] Cheng C.Z., Chen L. and Chance M.S. 1985 *Ann. Phys.* **161** 21
[5] Dewar *et al* 1974 *Phys. Fluids* **19** 930
[6] Kieras and Tataronis 1982 *J. Plasma Phys.* **28** 395
[7] Betti R. *et al* 1991 *Phys. Fluids* B **3** 1865
[8] Chen L. 1988 *Proc. Joint Varenna-Laussane Int Workshop on Theory of Fusion Plasmas (Chexbres, Switzerland, 3–7 October 1988)* ed J. Vaclavik, F. Troyon and E. Sindoni, p 327
[9] Fu G.Y. and Van Dam J.W. 1989 *Phys. Fluids* B **1** 1949
[10] Wong K.L. *et al* 1991 *Phys. Rev. Lett.* **66** 1874
[11] Ali-Arshad S. and Campbell D. 1995 *Plasma Phys. Control. Fusion* **37** 715
[12] Wilson *et al* 1993 *Int. Conf. Plasma Physics Cont. Fusion Research 1992: Proc. 14th Int. Conf. (Wurzburg, 1992)* vol 1 (Vienna: IAEA) p 661
[13] Saigusa *et al* 1995 *Plasma Phys. Control. Fusion* **37** 295
[14] Fasoli A. *et al* 1997 *Plasma Phys. Control. Fusion* **39** B287
[15] Kerner W. *et al* 1998 *Nucl. Fusion* **38** 1315
[16] Fasoli A. *et al* 1995 *Nucl. Fusion* **35** 1485
[17] Fasoli A. *et al* 1996 *Nucl. Fusion* **36** 258
[18] Hawkes N. *et al* 2001 *Phys. Rev. Lett.* **87** 115001
[19] Levinton F. *et al* 1989 *Phys. Rev. Lett.* **63** 2060
[20] Chen L. 1994 *Phys. Plasmas* **1** 1519
[21] Zonca F. and Chen L. 1996 *Phys. Plasmas* **3** 323
[22] Chen *et al* 1995 *Nucl. Fusion* **35** 1639
[23] Bernabei *et al* 1999 *Phys. Plasmas* **6** 1880
[24] Fasoli A. *et al* 1998 *Phys. Rev. Lett.* **81** 25
[25] Borba D. and Kerner W. 1999 *J. Comput. Phys.* **153** 101
[26] Berk H. *et al* 2001 *Phys. Rev. Lett.* **87** 18
[27] Candy J. *et al* 1996 *Phys. Lett.* A **215** 299
[28] Kerner W. *et al* 1998 *J. Comput. Phys.* **142** 271
[29] Huysmans G.T.A. *et al* 1993 *Phys. Fluids* B **5** 1545
[30] Connor J. *et al* 1994 *21th EPS Proc.* vol 18B (part II), p 616
[31] Vaclavik J. and Appert K. 1991 *Nucl. Fusion* **31** 1945
[32] Goedbloed J.P. 1975 *Phys. Fluids* **18** 1258
[33] Candy J. and Rosenbluth M.N. 1994 *Phys. Plasmas* **1** 356
[34] Borba D. *et al* 1994 *Phys. Plasmas* **1** 3151
[35] Mett R. and Mahajan S. 1992 *Phys. Fluids* B **4** 2885
[36] Jaun A. *et al* 1997 *Plasma Phys. Control. Fusion* **39** 549
[37] Nabais F. *et al* 2001 *Proc. European Conf. on Plasma Phys. and Control. Fusion (Funchal, 18–22 June 2001)* p 557
[38] Lao L. *et al* 1990 *Nucl. Fusion* **30** 1035
[39] Huysmans G.T.A *et al* 1992 *Phys. Fluids* B **3** 1506
[40] Sharapov S. *et al* 2001 *Phys. Lett.* A **289** 127